

# Subwavelength Plasma Gratings Formation in the Process of Laser Modification in the Volume of Fused Silica

Anna V. Bogatskaya<sup>1,2</sup><sup>a</sup>, Ekaterina A. Volkova<sup>3</sup><sup>b</sup> and Alexander M. Popov<sup>1,2</sup><sup>c</sup>

<sup>1</sup>*Department of Physics, Lomonosov Moscow State University, 119991, Moscow, Russia*

<sup>2</sup>*Lebedev Physical Institute, Russian Academy of Sciences, 119991, Moscow Russia*

<sup>3</sup>*Skobeltsyn Institute of Nuclear Physics, Lomonosov Moscow State University, 119991, Moscow, Russia*

**Keywords:** Laser Microstructuring in Dielectrics, Birefringent Nanolattices, Fused Silica, Multiphoton Ionization of Dielectrics, Plasma Formation, Numerical Modelling, Wave Equation.

**Abstract:** In this work, a numerical study of the formation of plasma periodic subwavelength nanogratings in fused silica along the propagation of a focused laser pulse is carried out. It is shown that the tightly focused beam creates a supercritical plasma in the focal plane, which provides an effective reflection of the parts of incident and reflected laser pulse. As a result, standing wave of ionization occurs which generates a plasma lattice with a period equal to the period of the standing wave in the medium. The results of modelling allow us to determine the optimal laser parameters in the regime of linear (geometrical) focusing when the contrast nanogratings can emerge. Analysis of energy release processes with subsequent melting of the fused silica sample confirms the previously proposed mechanism of laser modification.


## 1 INTRODUCTION


In recent decades, significant efforts have been dedicated to explore the intricate hierarchical processes involved in altering physical properties of materials exposed by highly focused femtosecond laser pulses (Gattass and Mazur, 2008; Taylor, et. al., 2007; Bulgakova, et. al., 2015). Advanced ultrafast laser facilities have uncovered new mechanisms underlying the interaction between electromagnetic fields, plasma, and materials. These interactions result in diverse structural changes in transparent dielectric materials, including the generation of micro- and nanoscale voids, densification zones and micro-tracks (Shimotsuma, et. al., 2005; Sun, et. al., 2007; Beresna, et. al., 2011; Dai, et. al., 2016; Mizeikis, et. al., 2009), periodic shifts in refractive indices (Schaffer, et. al., 2001; Wang, et. al., 2007; Mermillod-Blondin, et. al., 2008) etc.


Fused silica glass has garnered significant attention since the publication of a pioneering work (Shimotsuma, et. al., 2003) that initially introduced the concept of creating birefringent volume

nanogratings in this material. Subsequent studies by multiple scientific groups (Desmarchelier, et. al., 2015; Bulgakova, et. al., 2013) have unveiled several key mechanisms behind the formation of these structures. These mechanisms include the coupling of electron plasma waves with the incident light (Shimotsuma, et. al., 2005; Shimotsuma, et. al., 2003), the formation of nanoplasmas due to localized field enhancements and their self-organization into nanoscale patterns (Bhardwaj, et. al., 2006; Taylor, et. al., 2008), and the attractive interaction and rapid confinement of exciton-polaritons (Beresna, et. al., 2012).

More recently, a novel approach to forming volume nanogratings was introduced (Kudryashov, et. al., 2021; Kudryashov, et. al., 2022). According to the proposed mechanism the plasma stage of matter self-organization in the dielectric volume involves the following steps: (i) formation of highly reflective electron-hole plasma of near-critical density in the area of linear focus, (ii) longitudinal interference of the reflected and incident parts of linearly polarized femtosecond pulse in the pre-focal region, forming

<sup>a</sup> <https://orcid.org/0000-0002-1538-3433>

<sup>b</sup> <https://orcid.org/0000-0002-4883-3349>

<sup>c</sup> <https://orcid.org/0000-0002-7300-3785>

the near-plane standing electromagnetic wave and the corresponding ionization wave (plasma sheets) with the period  $\lambda/2n'$ , where  $\lambda$  is the wavelength of exposed laser radiation,  $n' = \text{Re}[\sqrt{\varepsilon(z)}]$  is the real part of plasma refractive index, (iii) excitation and interference of interfacial (at the boundary between weakly/strongly photoexcited dielectric layers) sub-wavelength plasmons, producing in each plasma sheet a periodic modification along the laser polarization with the period equal to half of the plasmon wavelength  $\Lambda_p/2 \sim \lambda/2n^2$ . The recent experimental studies (Kudryashov, et. al., 2022) have shown that better implementation of the proposed nanostructuring appears in a linear (pre-filamentary regime). However, despite a number of experimental studies, the assignment of nanopatterns to given laser focusing regimes (the dependence of such nanostructuring mechanism on the parameters of laser exposure in the linear focusing regime) remains not completely clear. In particular, the reproducibility of well written («contrast») periodic structures in a number of dielectric materials remains an important and unexplored issue. Thus, it seems relevant to develop rigorous numerical models to verify the proposed mechanism, as well as to more accurately predict the optimal parameters of focusing, duration, and intensity of laser radiation for the best realization of contrast nanostructures in the experiment.

In this work we perform a self-consistent numerical modelling of a focused subpicosecond laser pulse propagation in fused silica together with the generation and evolution of electron-hole plasma in order to verify the first step of the proposed mechanism (i.e. plasma gratings formation along the pulse propagation) for the parameters that are rather close to those in recent experiments (Kudryashov, et. al., 2022; Kudryashov, et. al, 2023). Our modelling shows that strong reflection occurs in the region of focal plane, which induces subsequent pulse reflection from the focal plasma with the formation of a series of plasma sheets in the pre-focal region. The conducted analysis enables to reveal the optimal laser parameters in the regime of linear (geometrical) focusing when the most distinct subwavelength plasma gratings can be generated.

## 2 MODELLING AND METHODS

According to the series of conducted experiments in fused silica (Kudryashov, et. al., 2022; Kudryashov, et. al, 2023) we choose pulses up to 1  $\mu\text{J}$  energy at 1030 nm wavelength and sub-femtosecond duration.

As in experiments the pulse repetition rate is low enough ( $\sim 100$  kHz) compared to the characteristic times of plasma diffusion and recombination, we can neglect the inter-pulse effects, thus considering the only intra-pulse dynamics laser induced solid-state plasma.

Wave equation for the field propagation of a linearly polarized pulse in a dielectric along  $z$  axis reads:

$$\nabla^2 E = \frac{\varepsilon(z)}{c^2} \frac{\partial^2 E}{\partial t^2} + \frac{4\pi}{c^2} \frac{\partial(j(z,t) + j_{ion}(z,t))}{\partial t}. \quad (1)$$

Here  $\varepsilon(z) = n_0^2 \cong 2.1$  is the dielectric permittivity of fused silica (we assume that there is no dispersion within the laser pulse spectrum width)  $n_0$  is the refractive index, and  $j$  is the current density created by electrons in the conduction zone,  $j_{ion}$  is the so-called ionization current due to the losses of field energy during ionization (transitions between the valence and the conduction zones). In general, equation (1) is two-dimensional and describes the focusing of the beam in some area inside the dielectric, where electrons arise as a result of multiphoton (or tunnel) ionization. We will solve the problem (1) in the quasi one-dimensional approximation (the validity of this approach will be analyzed later):

$$\frac{\partial^2 E(z,t)}{\partial z^2} = \frac{\varepsilon(z)}{c^2} \frac{\partial^2 E(z,t)}{\partial t^2} + \frac{4\pi}{c^2} \frac{\partial(j + j_{ion})}{\partial t}. \quad (2)$$

According to the initial conditions of the problem, the laser pulse is located on the grid in the region to the left of the focal region and moves towards it. The coordinate of the leading edge of the pulse  $z^*$  is such that the entire pulse is to the left of the focal plane. The pulse is characterized by a "sine-square" envelope:

$$\begin{aligned} E(z, t = 0) &= E_0 \sin^2\left(\frac{\pi(z - z^*)}{\ell}\right), \\ z &\in \{z^*, z^* + \ell\}; \\ E(z, t = 0) &= 0, z \notin \{z^*, z^* + \ell\}. \end{aligned} \quad (3)$$

Here  $\ell = 0.012$  cm is the length of the laser pulse which is determined by the base of the pulse. Such a pulse is rather close for the Gaussian pulse with the pulse duration  $\tau_p = 0.3$  ps (FWHM). Focusing of the laser pulse during its propagation was taken into account by multiplying the solution of equation (2) by the function  $F(z)$  which is a geometric factor determining the degree of beam broadening as it

moves away from the focal plane. We define this function by the expression

$$F(z - z_0) = 1 / \sqrt{1 + \left(\frac{z - z_0}{z_f}\right)^2}, \quad (4)$$

where  $z_0$  is the position of the focal plane,  $z_f$  is the beam focal length. In this case, the focused field  $\tilde{E}(z, t)$  at the point with coordinate  $z$  will be obtained via the solution (2) as

$$\tilde{E}(z, t) = E(z, t) \times F(z). \quad (5)$$

It is the field that will determine the birth and dynamics of electrons in the fused silica volume. The current  $j(z, t)$  in equation (2) will be determined within the framework of the Drude model:

$$j(z, t) + \nu_{tr} j(z, t) = \frac{e^2 n_e}{m^*} \tilde{E}(z, t). \quad (6)$$

Here  $\nu_{tr} \approx 3 \cdot 10^{13} \text{ s}^{-1}$  is the transport frequency of electron scattering in the conduction band (we do not take into account the effect of changing the transport frequency as a result of its heating),  $n_e$  is the electron concentration,  $m^* = 0.5m_e$  is the effective mass of electrons in fused silica ( $m$  is the mass of an electron). Equation (6) was solved at each node of the spatial grid where the function  $\tilde{E}(z, t)$  is defined. Here we also suppose that the number of electrons per field period is practically unchanged. To analyse the evolution of electron-hole plasma in the dielectric volume, the following equation is solved

$$\frac{\partial n_e}{\partial t} = D \frac{\partial^2 n_e}{\partial z^2} + W_i(I(z, t))(N_0 - n_e) + \nu_i(I) n_e \left(1 - \frac{n_e}{N_0}\right) - \frac{n_e}{\tau_r}, \quad (7)$$

where  $N_0 = 2.1 \times 10^{22} \text{ cm}^{-3}$  is the neutral atoms concentration,  $D$  is the electron diffusion coefficient which was estimated as  $D \sim \frac{v_f^2}{3\nu_{tr}} \approx 300 \text{ cm}^2/\text{s}$ , where  $V_f \approx 10^8 \text{ cm/s}$  is the Fermi speed,  $\tau_r = 150 \text{ fs}$  is the mean recombination time in fused silica (Audebert, et. al., 1990),  $W_i(I(z, t))$  is the rate of ionization in fused silica calculated using the Keldysh formula (Bogatskaya, et. al., 2023),  $\nu_i(I) = \frac{1}{I_i} \frac{4\pi e^2 I(z, t) \nu_{tr}}{c n_0 m^* (\omega^2 + \nu_{tr}^2)}$  is the frequency of impact ionization. In expression  $\nu_i(I)$  one should set:  $I_i = 9 \text{ eV}$  which is a value of bandgap in fused silica,  $\omega$  is the frequency of laser radiation. It is worth noting that the radiation intensity appearing in the expressions of multiphoton

(Keldysh) and impact ionization is calculated as  $I(z, t) = \langle \frac{c}{4\pi} n_0 \tilde{E}(z, t)^2 \rangle$ , where brackets mean averaging over the period of oscillation of the wave field. The ionization current used in equation (2) can be written as

$$j_{ion} = \frac{I_i}{\langle E \rangle} \frac{dn_e}{dt} = \frac{I_i}{E} W_i(I(z, t))(N_0 - n_e), \quad (8)$$

where  $\langle E \rangle$  is an averaged over the period field  $\tilde{E}(z, t)$ .

### 3 RESULTS AND DISCUSSION

Below we perform simulations for the following laser beam parameters (see Table 1). In particular, we choose the values of focal waists corresponding to the focusing of  $\lambda = 1030 \text{ nm}$  laser pulse by micro-objective lenses with different values of numerical aperture  $NA = 0.65, 0.55, 0.25$  which are available at laser workstation based on the femtosecond Yb-doped fiber laser Satsuma (Amplitude Systems, Pessac, France) with the fundamental wavelength  $\lambda = 1030 \text{ nm}$  used in Lebedev Physical Institute RAS for corresponding experiments on laser misstructuring (Kudryashov, et. al., 2021; Kudryashov, et. al., 2022; Kudryashov, et. al., 2023). The intensity range in simulations is also determined by pulse energies and durations available in the experiments in the pre-filamentary regime. Recent analysis carried out in (Bogatskaya, et. al., 2023) has demonstrated that the intensity range required for effective ionization of a sample lies in the range of 10-100 TW/cm<sup>2</sup>. It is worth noting here that, based on the data in Table 1, the spatial pulse length  $\ell \gg z_f$ , which makes the quasi-one-dimensional approximation acceptable for analyzing the propagation of the pulse wave field in the near-focal region.

Table 1: Focused laser parameters.

$I = 10 \div 100 \text{ TW/cm}^2$ (peak intensity of the pulse)
$\ell = 0.012 \text{ cm}$
$z_f \sim 2-30 \text{ }\mu\text{m}$
$z_0 = 0.045 \text{ cm}$
$z^* = 0.0216 \text{ cm}$

Let us start with the data on plasma density profiles formed in the near focal region for  $z_f = 2 \text{ }\mu\text{m}$  (this corresponds to tight focusing conditions:  $NA \sim 0.25$ ) for different values of laser intensity (Figure 1). The profiles of plasma structures demonstrate the appearance of periodicity with increasing pulse

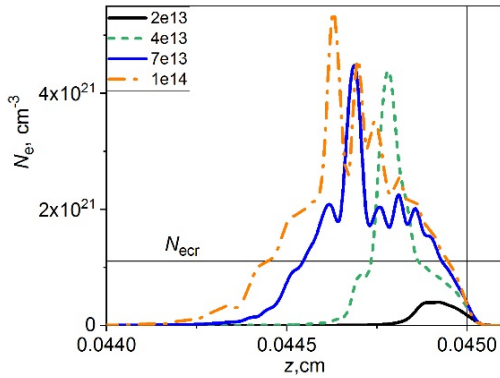


Figure 1: Plasma density profiles formed along the laser pulse propagation in the pre-focal region for different peak pulse intensities in  $\text{W}/\text{cm}^2$  (see the plot legend). The value of focal waist  $z_f = 2 \mu\text{m}$ . The instant of time ( $t = t_f$ ) approximately corresponds to the focusing of the central part of the beam. The vertical grid line corresponds to the position of focal plane. Horizontal grid indicates the value of critical electron density ( $N_{ecr} = 1.1 \times 10^{21} \text{ cm}^{-3}$ ).

intensity. In addition, with increasing intensity, the region of high ionization of the medium increases, leading to supercritical electron concentrations and, as a consequence, effective reflection of the laser pulse. It is also worth noting that the formation of structures occurs in the pre-focal region. To verify the proposed idea of nanograting formation, based on the pulse reflection from the focal plasma, we present data on the wave field of the pulse at different times (Figure 2). One can see that the area of effective interaction of the incident and reflected parts of the laser pulse occurs in the pre-focal region, while the transmitted through the focal plane part turns out to be insignificant for plasma formation.

It is worth noting that the spatial length of the periodic plasma formation in the direction of laser pulse propagation, in addition to the intensity, will also be determined by the value of the focal waist. For further analysis of the dependence of plasma grating formation on the laser focusing length we present the simulations of plasma density for the value of the focal waist  $z_f = 7.2 \mu\text{m}$  (see Figure 3). Comparing the electron density profiles presented in Figures 1 and 3, it is appropriate to conclude that by increasing the size of the focal waist, we thereby increase the spatial area of effective ionization by a standing wave formed during pulse reflection. On the other hand, as  $z_f$  increases, one simultaneously observes a drop in the maximum concentration level, which, in turn, worsens the reflection coherence and leads to decrement in the contrast of structures (the difference in the degree of ionization at the nodes and antinodes of the standing wave).

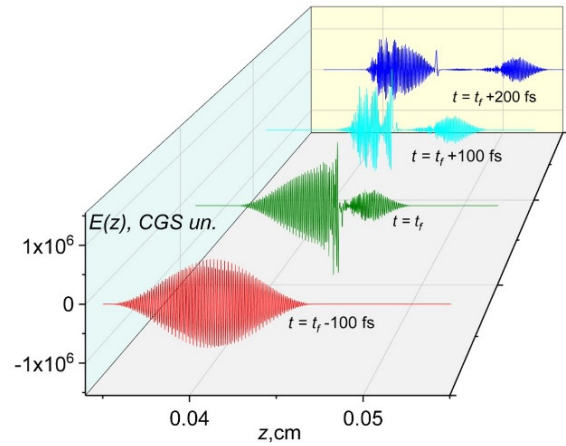


Figure 2: Pulse propagation for different instants of time ( $t_f$  corresponds to the moment of focusing of the central part of the pulse). Peak intensity is  $70 \text{ TW}/\text{cm}^2$ .

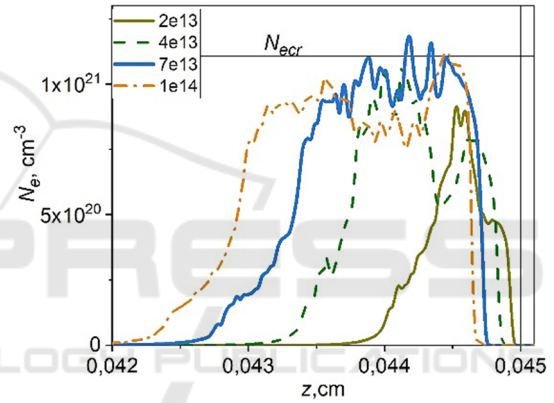


Figure 3: Plasma density profiles formed along the laser pulse propagation in the pre-focal region for different peak pulse intensities in  $\text{W}/\text{cm}^2$  (see the plot legend). The value of focal waist  $z_f = 7.2 \mu\text{m}$ . The instant of time is equal to  $t_f + 100 \text{ fs}$  (instant of time at which the maximum electron concentration in plasma gratings is reached). The vertical grid line corresponds to the position of focal plane. Horizontal grid indicates the value of critical electron concentration ( $N_{ecr} = 1.1 \times 10^{21} \text{ cm}^{-3}$ ).

Thus, further increase of the focal waist length in a given range of intensities does not ensure the achievement of sufficient electron concentrations, as a consequence, the periodicity of plasma lattices is washed out (see Fig. 4). Importantly, in this case the formation of plasma occurs in the region of space farther from the focal plane, thus most of the pulse is absorbed in the pre-focal region and does not reach the focusing plane.

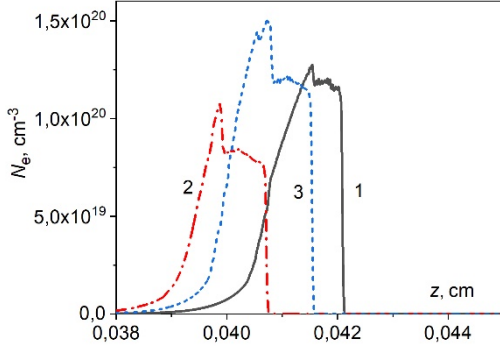


Figure 4: Plasma density profiles formed along the laser pulse propagation in the pre-focal region for different peak pulse intensities (in  $\text{W}/\text{cm}^2$ ): 1)  $2 \cdot 10^{13}$ , 2)  $3 \cdot 10^{13}$ , 3)  $5 \cdot 10^{13}$ . The value of focal waist  $z_f = 30 \mu\text{m}$ . The instant of time is the same as in Fig. 1.

Based on the analysis of simulation data, there exist the optimal focusing parameters at which it is possible to realize the most contrasting plasma lattice profiles within the proposed mechanism. Figure 5 shows the dependence of plasma absorption versus the length of the focal waist for three values of pulse peak intensity. One can see that the highest absorption in plasma can be reached for  $z_f \sim 5 - 10 \mu\text{m}$ . Indeed, a shortening of the focal waist leads to a reduction of the region of high ionization and, as a consequence, pulse absorption drops; on the other hand, a significant increase of  $z_f$  results in smoother dynamics of the pulse absorption during propagation, which in turn worsens the process of its effective reflection in the focusing zone. As was mentioned, the contrast of plasma gratings is determined by the degree of coherence of the incident and reflected parts of the pulse, which turns out to be easier to implement with tighter focusing conditions.

In conclusion, we would like to note that the process of further modification of the dielectric material is associated with the processes of heat transfer and subsequent melting of the sample, which will differ in intensity in the regions of weak and strong sample ionization. Below we give qualitative estimates of the processes of heating and melting of the sample. From the data in Figure 5, we can see that the maximum fraction of absorbed energy in the ionization process is  $\sim 60\%$ . Assuming that the initial pulse energy is  $\sim 0.5 \mu\text{J}$  ( $0.1-1 \mu\text{J}$  according to the experiments (Kudryashov, et. al., 2021; Kudryashov, et. al., 2022; Kudryashov, et. al, 2023)), the absorbed energy can be estimated as  $Q_a \approx 0.3 \mu\text{J}$ . Here we suppose that the main contribution to the energy absorption is made by the process of photoionization of electrons. The energy required to heat the substance to the melting temperature can be estimated as:

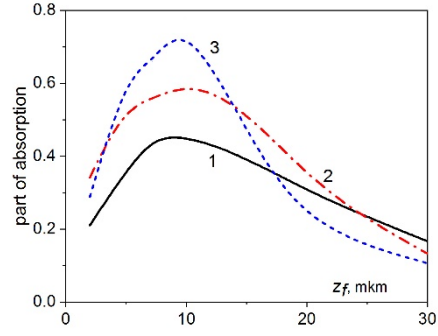


Figure 5: Plasma absorption versus the focal waist length for different peak intensities of laser radiation (in  $\text{W}/\text{cm}^2$ ): 1)  $2 \cdot 10^{13}$ , 2)  $3 \cdot 10^{13}$ , 3)  $5 \cdot 10^{13}$ .

$$\Delta Q = C \cdot M \cdot \Delta T \approx 0.15 \mu\text{J}, \quad (9)$$

where  $C = 1.05 \text{ J}/(\text{g K})$  is the specific thermal capacity of silica,  $M$  is the mass of laser exposed substance and  $\Delta T$  is the difference between initial temperature and temperature of melting ( $T_{\text{melt}} \approx 2000 \text{ K}$  [29]) from the room temperature  $T_0 = 300 \text{ K}$ .

We estimate the mass  $M$  as  $M \cong \rho \cdot \int_{z_0 - \frac{z_f}{2}}^{z_0 + \frac{z_f}{2}} S_0 \cdot F(z - z_0)^{-2} dz$  with  $\rho = 2.2 \text{ g}/\text{cm}^3$  to be the fused silica density and the beam area in the focal waist  $S_0$ . For typical values from the experiment (Kudryashov, et. al., 2022; Kudryashov, et. al, 2023)  $S_0 \approx 10^{-4} \mu\text{m}^2$  and  $z_f = 7.2 \mu\text{m}$  one obtains  $M \approx 10^{-10} \text{ g}$ . The energy required to melt a substance heated to the melting point can be estimated via the expression:

$$\Delta Q_m = L \cdot M \approx 0.01 \mu\text{J}. \quad (10)$$

Here  $L = 140 \text{ J}/\text{g}$  is the heat of melting in fused silica. Thus, the above estimates show that the absorbed energy  $Q_a$  is sufficient for heating with the subsequent the formation of melting zones leading to residual modification of the fused silica sample. The melted regions after the sample cooling will be characterized by a modified refractive index which will differ from the initial value  $n_0$  by an amount of the order of  $\Delta n \sim 10^{-3}$  which is confirmed by recent experiments (Kudryashov, et. al., 2021; Kudryashov, et. al., 2022; Kudryashov, et. al, 2023).

## 4 CONCLUSIONS

To conclude, a numerical analysis was conducted to investigate the focused femtosecond laser radiation exposure on solid dielectric materials. The aim was to verify the proposed model that describes the formation of plasma sheets during the reflection of

laser pulse from the focal plasma with supercritical electron concentration. The obtained results allow us to identify the specific laser focusing conditions necessary for this regime of material nanostructuring. Notably, the research has revealed that the formation of contrast plasma lattices requires a tightly focused laser conditions. These findings represent a crucial step in comprehending the intricate mechanisms involved in modifying solids and the underlying physical processes. It brings us closer to the development of an advanced theoretical model that will enhance our ability to precisely control microscale laser modifications in solid dielectric materials.

## ACKNOWLEDGEMENTS

This research was funded by the Russian Science Foundation (project no. 22-72-10076).

## REFERENCES

- Gattass, R., Mazur, E. (2008). *Nature Photon*, 2, 219–225.
- Taylor, R. S., Hnatovsky, C., Simova, E., Pattathilet, R. (2007). *Optics Letters*, 32 (19), 2888-2890.
- Bulgakova, N. M.; Zhukov, V. P.; Sonina, S. V.; Meshcheryakov, Y.P. (2015). *J. Appl. Phys.*, 118 (23), 233108.
- Shimotsuma, Y.; Hirao, K.; Qiu, J. R.; Kazansky, P. G. (2005). *Modern Phys. Lett. B*, 19, 225.
- Sun, H.Y.; Song, J.; Li, C.B.; Xu, J.; Wang, X. S.; Cheng, Y.; Xu, Z. Z.; Qiu, J. R.; Jia, T. (2007). *Appl. Phys. A*, 88, 285.
- Beresna, M.; Gecevičius, M.; Bulgakova, N. M.; Kazansky, P. G. (2011). *Opt. Express*, 19, 18989.
- Dai, Y.; Patel, A.; Song, J.; Beresna, M.; and Kazansky, P. G. (2016). *Opt. Express*, 24, 19344
- Mizeikis, V.; Juodkazis, S.; Balciunas, T.; Misawa, H.; Kudryashov, S.I.; Ionin, A.A.; Zvorykin, V.D. (2009). *J. Appl. Phys.*, 105, 123106.
- Schaffer, C. B.; Brodeur, A.; García, J. F.; Mazur, E. (2001). *Opt. Lett.*, 26, 93.
- Wang, Z.; Sugioka, K.; Hanada, Y.; Midorikawa, K. (2007). *Appl. Phys. A*, 88, 699.
- Mermillod-Blondin, A.; Burakov, I. M.; Meshcheryakov, Y. P.; Bulgakova, N. M.; Audouard, E.; Rosenfeld, A.; Husakou, A.; Hertel, I. V.; Stoian, R. (2008). *Phys. Rev. B*, 77, 104205
- Shimotsuma, Y.; Kazansky, P. G.; Qiu, J. R.; Hirao, K. (2003). *Phys. Rev. Lett.*, 91, 247405.
- Desmarchelier, R.; Poumellec, B.; Brisset, F.; Mazerat, S. and Lancry, M. (2015). *World Journal of Nano Science and Engineering*, 5, 115-125.
- Bulgakova, N. M.; Zhukov, V. P.; Meshcheryakov, Yu. P. (2013). *Appl. Phys. B*, 113(3), 437-449.
- Bhardwaj, V. R.; Simova, E.; Rajeev, P. P.; Hnatovsky, C.; Taylor, R. S.; Rayner, D. M.; Corkum, P.B. (2006). *Phys. Rev. Lett.*, 96, 057404.
- Taylor, R.; Hnatovsky, C.; Simova, E. (2008). *Laser Photonics Rev.*, 2, 26.
- Beresna, M.; Gecevičius, M.; Kazansky, P. G.; Taylor, T.; Kavokin, A. (2012). *A. Appl. Phys. Lett.*, 101, 053120.
- Kudryashov, S. I.; Danilov, P. A.; Smaev, M. P.; Rupasov, A. E.; Zolot'ko, A. S.; Ionin, A. A.; Zakoldaev, R. A. (2021). *JETP Lett.*, 113, 493-497.
- Kudryashov, S.; Rupasov, A.; Kosobokov, M.; Akhmatkhanov, A.; Krasin, G.; Danilov, P.; Lisjikh, B.; Abramov, A.; Greshnyakov, E.; Kuzmin, E.; et al. (2022). *Nanomaterials*, 12, 4303.
- Kudryashov, S.; Rupasov, A.; Smayev, M.; Danilov, P.; Kuzmin, E.; Mushkarina, I.; Gorevoy, A.; Bogatskaya, A.; and Zolot'ko, A. (2023) *Nanomaterials*, 13(6), 1133.
- Audebert, P.; Daguzan, Ph.; Dos Santos, A.; Gauthier, J. C.; Geindre, J. P.; Guizard, S.; Hamoniaux, G.; Krastev, K.; Martin, P.; Petite, G.; and Antonetti, A. (1994). *Phys. Rev. Lett.*, 73 (14), 1990.
- Bogatskaya, A.; Gulina, Yu.; Smirnov, N.; Gritsenko, I.; Kudryashov, S.; and Popov, A. (2023). *Photonics*, 10, 515.